Free Vibration Analysis of Curvilinearly Tapered Axially Functionally Graded Material Beams

Vyacheslav N. Burlayenko *, Reijo Kouhia, Svetlana D. Dimitrova

Posted Date: 12 July 2024

doi: 10.20944/preprints202407.0993.v1

Keywords: free vibrations; axially functionally graded material; curvilinear tapered beam; differential transform method; ABAQUS

Article

Free Vibration Analysis of Curvilinearly Tapered Axially Functionally Graded Material Beams

Vyacheslav N. Burlayenko [1,*], Reijo Kouhia [2] and Svetlana D. Dimitrova [3]

[1] Department of Applied Mathematics, National Technical University 'KhPI', 2 Kyrpychova Str., Kharkiv 61002, Ukraine
[2] Faculty of Built Environment, Tampere University, POB 600, 33101 Tampere, Finland; reijo.kouhia@tuni.fi
[3] Department of Higher Mathematics, National Technical University 'KhPI', 2 Kyrpychova Str., Kharkiv 61002, Ukraine; s.dimitrovaburlayenko@gmail.com
* Correspondence: burlayenko@yahoo.com

Abstract: The study focuses on the free vibration analysis of beams made of axially functionally graded materials (AFGM) with curvilinear variable cross-sections along their length. The beams encompass various shapes, including concave and convex conic sections, with axial material properties varying according to polynomial and exponential laws. The equations of motion are derived using Hamilton's principle within the framework of Timoshenko beam theory. These governing equations, subjected to various boundary conditions, are solved using the differential transform method (DTM). The proposed solution technique is validated by comparing computed natural frequencies with existing in literature results and those obtained through three-dimensional finite element analysis in ABAQUS. The incorporation of material gradients into the beam finite element models was achieved through the user-defined material subroutine (UMAT). Additionally, a comprehensive study is conducted to examine the influence of various factors on the natural frequencies of functionally graded beams. These factors include parameters of material laws, types of variable beam shapes, slenderness ratio, and specific boundary conditions. This study provides a thorough understanding of the modal dynamics of the considered beams, offering valuable insights into the behavior of FGM structures.

Keywords: free vibrations; axially functionally graded material; curvilinear tapered beam; differential transform method; ABAQUS

1. Introduction

Incorporating variable cross-sections in structural elements facilitates achieving an optimal balance between weight and strength, especially in critical applications like helicopter blades, airplane propellers, turbine blades, and wind turbines. Given their significance, there has been extensive research on the vibrations of these structures, often modeled as beams with variable cross-sections [1–3].

The increasing use of functionally graded materials (FGMs) in beam-like structures underscores the need to account for material variations. FGMs enhance performance and provide a continuous stress distribution, unlike the discontinuities found in laminated and sandwich composites [4–6].

While initial research focused on material gradients in the thickness direction, there is significant interest in longitudinally graded materials, known as axially functionally graded material (AFGM) structures. Analyzing the free vibration of non-uniform AFGM beams involves recognizing that the coefficients in the equations of motion, derived from any beam theory, vary with changes in cross-sections and material properties along the beam's length. Consequently, solving these differential equations is not straightforward and often necessitates numerical procedures.

In the context of one-dimensional continuous models with inhomogeneous material parameters, Elishakoff and co-workers have presented exact solutions for the fundamental frequency of diverse AFG beams with different end supports [7]. Yuan et al. (2016) [8] applied the confluent hypergeometric function method to obtain exact solutions for Timoshenko beams with varying bending stiffness. Zhao et al. (2017) [9] employed the Chebyshev polynomials theory to analyze the

 doi:10.20944/preprints202407.0993.v1

free vibration of both AFGM Euler–Bernoulli and Timoshenko beams with non-uniform cross-sections. Xie et al. (2017) [10] exploited the spectral collocation method to examine the statics and free vibrations of Euler–Bernoulli beams with axially variable cross-sections and material parameters, while Chen (2021) [11] extended this technique to non-uniform AFG Timoshenko beams. Additionally, Zhang et al. (2019) [12] utilized a Jacobi polynomial-based approximation, and Cao et al. (2019) [13] used the asymptotic perturbation method for vibrational analysis of non-uniform AFGM beams.

Other researchers have creatively adapted methods known from studying homogeneous beams with variable cross-sections to address solutions for non-uniform AFGM beams. For instance, Ghazaryan et al. (2018) [14] employed the differential transform method to study the free vibration characteristics of AFGM Euler-Bernoulli beams, while Rajasekaran and Tochaei (2014) [15] used both the differential transform element and differential quadrature element methods to study AFGM Timoshenko beams, both with varying cross-sectional profiles and material properties along the beam axis. Keshmiri et al. (2018) [16] determined natural frequencies of cantilever beams with different variable cross-sections and material gradients using the Adomian decomposition method (ADM), and Lin et al. (2022) [17] investigated the vibration of rotating non-uniform AFG Euler–Bernoulli beams using the Laplace ADM. In turn, Wang et al. (2022) [18] combined ADM with an iterative process for reliability analysis of composite beams with varying cross-section rigidities and mass distributions along their length. Mahmoud (2019) [19] presented a general solution for the free transverse vibration of cantilever non-uniform AFGM Euler-Bernoulli beams, loaded at the tips with point masses, using the Myklestad method. Chen et al. (2021) [20] employed the variational iteration method to determine the modal characteristics of tapered AFGM Euler–Bernoulli and Timoshenko beams. Liu et al. (2022) [21] proposed a closed-form dynamic stiffness formulation for free vibration analysis of tapered and/or FGM Euler–Bernoulli beams. Adelkhani and Ghanbari (2022) [22] analyzed the vibrations of tapered AFGM beams with nonlinear profiles using the point collocation method.

To investigate the dynamics of AFGM tapered beams under large deflection scenarios, Kumar et al. (2015) [23] employed the Rayleigh-Ritz method with start functions derived from nonlinear static analysis within the Euler-Bernoulli beam theory with von Kármán geometric nonlinearity, while Ghayesh (2018) [24] utilized the Galerkin method and the third-order shear deformation beam theory. Soltani and Asgarian (2019) [25] developed a hybrid approach combining the power series expansions and the Rayleigh-Ritz method for stability and free vibration analyses of non-uniform AFGM beams resting on Winkler-Pasternak elastic foundation. Singh and Sharma (2022) [26] carried out a vibration analysis of an AFGM non-prismatic Timoshenko beam under axial thermal variation in a humid environment using the harmonic differential quadrature method.

Finite element method-based approaches, tailored for precise and efficient study of this task, have also been proposed. Özdemir (2022) [27] studied free vibration and buckling characteristics of AFGM tapered rotating Euler–Bernoulli and Timoshenko beams with different end conditions using a two-noded beam element. Bazoune (2024) [28] proposed a Fourier-p element model for accurate predictions of Timoshenko-Ehrenfest beam frequencies with high precision compared to other existing models. Chen et al. (2019) [29] presented isogeometric analysis (IGA) in conjunction with elasticity theory for the three-dimensional vibration problem of AFGM beams with variable thickness. Murillo et al. [30] used the seven-parameter spectral finite element formulation to perform the analysis of FG shells of either uniform or non-uniform thickness. Burlayenko et al. (2024) [31] conducted simulations on the free vibrations of AFGM beams with non-uniform cross-sections, utilizing both one-dimensional and three-dimensional AFG finite element models developed in ABAQUS via user-defined subroutines [32–34].

Most of the examined non-uniform beams had rectangular cross-sections with linear taper. There were also studies on beams with parabolic and exponential thickness and constant or linear varying width, but less common. In some cases, vibrations of beams were investigated in scenarios such as truncated beams, beams with one sharp end, and beams with both ends sharp, as discussed in [1,3]. However, research on AFGM beams having arbitrary cross-section variations remains limited. Recently, Lee and Lee (2022) [35] studied the coupled flexural-torsional free vibration of circular horizontally curved beams with rectangular and elliptical cross-sections made of AFGMs

 doi:10.20944/preprints202407.0993.v1

with quadratic functions of Young's modulus and the mass density, using the trial eigenvalue method and numerical integration within the Timoshenko and Saint-Venant beam theories. Rezaiee-Pajand et al. (2022) [36] proposed a closed-form solution for the lateral-torsional buckling moment of a bidirectional exponentially functionally graded monosymmetric C-shaped Euler–Bernoulli beam. Liu et al. (2024) [37] presented a nonlinear model to obtain the mode shape and frequency of FGM Euler-Bernoulli thin-walled beams with varying cross-sections, employing the perturbation approach and the Galerkin method. Other researchers have explored the concept of transforming the equations of motion of non-uniform FGM beams into those of equivalent uniform beams. For instance, Chen et al. (2017) [38] applied this idea to a specific class of non-uniform FGM beams. Additionally, Martin and Salehian (2020) [39] developed a method based on metric minimization, modal participation factor and the proper orthogonal decomposition to accurately approximate a Euler-Bernoulli motion equation with spatially varying coefficients with an equivalent constant coefficient model.

The literature search indicates that studying the dynamics of tapered AFGM beams involves complexities. While various techniques have been reported, closed-form solutions are limited to specific cross-sections, material variations and defined boundary conditions. Numerical methods like FEM are proficient but make it challenging to derive general conclusions about system behavior [40]. In this respect, accurate semi-analytical approaches can be a good alternative. Despite extensive research, the vibration characteristics of AFGM beams with arbitrary continuously variable cross-sections are not fully addressed. This study aims to use the differential transform method (DTM) to obtain accurate semi-analytical solutions for the free vibration of curvilinearly tapered AFGM beams under various boundary conditions, determining the effects of variable cross-sections on natural frequencies and mode shapes. This is an innovation of the present contribution.

2. AFGM Beams with Variable Cross-Section

2.1. Geometry of the Beams

Focusing on the closed-form solution of the free vibration problem, we aim to describe various non-uniform beam geometries in a unified analytical manner. One effective way to achieve this is by using rational Bézier curves [41].

We consider planar beams of length of L that are symmetrical about their midlines, with the left ends positioned at the origin of the Cartesian coordinate system as shown in Figure 1. The top curve of these beams is a conic arc, represented by an algebraic quadratic equation in $\mathbb{R}^2$ as follows:

$$Ax^2 + Bxy + Cx^2 + Dx + Ey + F = 0. \tag{1}$$

The coefficients of (1) can be derived from the quadratic rational Bézier curve, which involves the control points $P_0(x_0; y_0)$, $P_1(x_1; y_1)$, $P_2(x_2; y_2)$ and the weight w_1, by utilizing the Gröbner basis as presented in [42]:

$$\begin{aligned}
A &= y_0^2 - 4w_1^2y_0y_1 + 4w_1^2y_1^2 - 2y_0y_2 + 4w_1^2y_0y_2 - 4w_1^2y_1y_2 + y_2^2,\\
B &= -2x_0y_0 + 4w_1^2x_1y_0 + 2x_2y_0 - 4w_1^2x_2y_0 + 4w_1^2x_0y_1 - 8w_1^2x_1y_1 + 4w_1^2x_2y_1 + 2x_0y_2\\
&\quad - 4w_1^2x_0y_2 + 4w_1^2x_1y_2 - 2x_2y_2,\\
C &= x_0^2 - 4w_1^2x_0x_1 + 4w_1^2x_1^2 - 2x_0x_2 + 4w_1^2x_0x_2 - 4w_1^2x_1x_2 + x_2^2,\\
D &= -2x_2y_0^2 + 4w_1^2x_1y_0y_1 + 4w_1^2x_2y_0y_1 - 4w_1^2x_0y_1^2 - 4w_1^2x_2y_1^2 + 2x_0y_0y_2 - 8w_1^2x_1y_0y_2\\
&\quad + 2x_2y_0y_2 + 4w_1^2x_0y_1y_2 + 4w_1^2x_1y_1y_2 - 2x_0y_2^2,\\
E &= -4w_1^2x_1^2y_0 + 2x_0x_2y_0 + 4w_1^2x_1x_2y_0 - 2x_2^2y_0 + 4w_1^2x_0x_1y_1 - 8w_1^2x_0x_2y_1 + 4w_1^2x_1x_2y_1\\
&\quad - 2x_0^2y_2 + 4w_1^2x_0x_1y_2 - 4w_1^2x_1^2y_2 + 2x_0x_2y_2,\\
F &= x_2^2y_0^2 - 4w_1^2x_1x_2y_0y_1 + 4w_1^2x_0x_2y_1^2 + 4w_1^2x_1^2y_0y_2 - 2x_0x_2y_0y_2 - 4w_1^2x_0x_1y_1y_2 + x_0^2y_2^2.
\end{aligned} \tag{2}$$

For convenience, let l_f and l_e denote the length of lines $\boldsymbol{P}_1\boldsymbol{P}_m$ and $\boldsymbol{P}_s\boldsymbol{P}_m$, respectively, where $\boldsymbol{P}_S = (1-s)\boldsymbol{P}_m + s\boldsymbol{P}_1$ is the shoulder point, $\boldsymbol{P}_m$ is the midpoint of line $\boldsymbol{P}_0\boldsymbol{P}_2$ and $s = \frac{l_e}{l_f}$ is a shape parameter related to $w_1 = \frac{s}{1-s}$. By specifying the coordinates of the points $\boldsymbol{P}_0$, $\boldsymbol{P}_1$, $\boldsymbol{P}_2$ and the

 doi:10.20944/preprints202407.0993.v1

parameter s, the implicit equation of a conic curve (1) can be constructed. The curve will have a convex upward shape if the vertex $\boldsymbol{P}_1$ is above the line $\boldsymbol{P}_0\boldsymbol{P}_2$, and a concave downward shape if $\boldsymbol{P}_1$ below the line $\boldsymbol{P}_0\boldsymbol{P}_2$ as illustrated in Figure 1a and b, respectively.

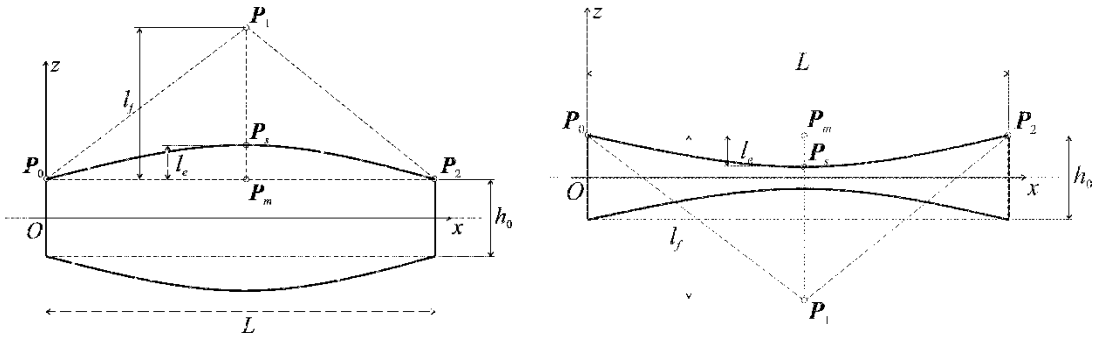

Figure 1. The geometries of AFGM beams with variable thickness: (**a**) Convex upward shape; (**b**) Concave downward shape.

2.2. Graded Materials of the Beams

We suppose that the materials of the beams with variable thickness are homogeneous in the thickness direction but graded along the axial direction. Consequently, the material properties, such as mass density and Young's modulus, vary with the position along the x-axis. Specifically, we analyze the following types of material distributions:

Type 1. The effective mass density and Young's modulus are power-law functions of x written as

$$\rho(x) = \rho_0 \sum_{i=0}^{m} a_i \left(\frac{x}{L}\right)^i, \qquad E(x) = E_0 \sum_{i=0}^{n} b_i \left(\frac{x}{L}\right)^i, \tag{2}$$

where ρ_0 and E_0 are the mass density and Young's modulus at $x = 0$, respectively; m and n are power coefficients that account for arbitrary variations of the material parameters along the beam's length; a_i and b_i constant coefficients.

Type 2. The effective density and Young's modulus follow exponential law functions of x, given by

$$\rho(x) = \rho_0 V_e, \; E(x) = E_0 V_e, \tag{3}$$

where the exponential function $V_e = e^{\gamma_e\left(1-a\left(1-\frac{x}{L}\right)\right)}$ is determined by the parameter a and gradation index γ_e, [29].

Type 3. The beams with variable thickness are composed of a metal-ceramic mixture. The effective material properties are calculated based on the rule of mixtures in the form:

$$\rho(x) = \rho_c + (\rho_m - \rho_c)V_c, \; E(x) = E_c + (E_m - E_c)V_c, \tag{4}$$

where the subscripts 'm' and 'c' refer to the properties of metal and ceramic constituents, respectively; V_c denotes the ceramic volume fraction, expressed as $V_c = \left(1 - b\left(1 - \frac{x}{L}\right)\right)^{\gamma_c}$ with the parameter b and gradation index γ_c, [29].

Poisson's ratio, ν is assumed to be constant throughout this study.

2.3. Governing Equations of the Beams

We consider the transverse vibrations of an AFGM beam in the xz-plane using the Timoshenko beam theory. The equations of motion governing such beams with generally variable cross-sections, in terms of the transverse displacement $w(x,t)$ of the midline and the cross-sectional rotation angle $\varphi(x,t)$ at time t are written as follows:

 doi:10.20944/preprints202407.0993.v1

$$-\frac{\partial}{\partial x}\left(D_{11}(x)\frac{\partial \varphi}{\partial x}\right)-A_{55}(x)\left(\frac{\partial w}{\partial x}-\varphi\right)+I_2(x)\frac{\partial^2\varphi}{\partial t^2}=0,$$
$$-\frac{\partial}{\partial x}\left(A_{55}(x)\left(\frac{\partial w}{\partial x}-\varphi\right)\right)+I_0(x)\frac{\partial^2 w}{\partial t^2}=0. \tag{5}$$

The rigidities and the inertia coefficients are expressed as integrals over the cross-sectional domain in the form:

$$D_{11}(x)=\int_{A(x)} z^2E(x)\,dA,\ A_{55}(x)=\kappa\int_{A(x)} G(x)\,dA,$$
$$(I_0(x),I_2(x))=\int_{A(x)}(1,z^2)\rho(x)\,dA, \tag{6}$$

where $\rho(x)$ is the mass density, $G(x)=\frac{E(x)}{2(1+\nu)}$ is the shear modulus and κ is the shear correction factor. Throughout this study, the shear factor is accepted as 5/6 unless specified otherwise.

Assuming simple harmonic oscillations, the deflection and the rotation angle can be expressed as

$$w(x,t)=\bar{w}(x)e^{i\omega t},\ \varphi(x,t)=\bar{\varphi}(x)e^{i\omega t}, \tag{7}$$

where $\bar{w}(x)$ and $\bar{\varphi}(x)$ are the amplitudes of the displacement and rotation angle, respectively, ω is the angular frequency; and $i^2=-1$ represents the imaginary unit.

Substituting (7) into (5) yields a system of coupled ordinary differential equations that describe the free transverse vibrations of a Timoshenko beam with a non-uniform cross-section as

$$\frac{d}{dx}\left(D_{11}(x)\frac{d\bar{\varphi}}{dx}\right)+A_{55}(x)\left(\frac{d\bar{w}}{dx}-\bar{\varphi}\right)+I_2(x)\omega^2\bar{\varphi}=0,$$
$$\frac{d}{dx}\left(A_{55}(x)\left(\frac{d\bar{w}}{dx}-\bar{\varphi}\right)\right)+I_0(x)\omega^2\bar{w}=0. \tag{8}$$

Herewith, the rigidities and inertia coefficients (6) can be conveniently presented by the expressions:

$$D_{11}(x)=E(x)I(x),\ A_{55}(x)=\kappa G(x)A(x),$$
$$I_0(x)=\rho(x)A(x),\ I_2(x)=\rho(x)J(x), \tag{9}$$

where $A(x)$ and $J(x)$ are the area and second inertia moment of the cross-section, respectively.

3. Solution Methodology

3.1. Differential Transform Method

Due to the variable coefficients, reflecting the dependence of material properties and cross-sectional geometry on the x-coordinate, the coupled nature of the differential equations in (8) presents mathematical challenges for finding a closed-form solution. To address this, we employ the differential transform method (DTM) for its versatility and simplicity. This method converts the differential equations into a set of recurrent algebraic equations, enabling the solution to be represented as an infinite power series. The fundamental aspects of the DTM can be found in G.E. Pukhov's original publications [43].

We reformulate system (8) a more suitable form for applying the DTM as follows:

$$\frac{d^2\bar{\varphi}}{dx^2}+\bar{D}_1(x)\frac{d\bar{\varphi}}{dx}+\bar{D}_2(x)\frac{d\bar{w}}{dx}-\bar{D}_2(x)\bar{\varphi}+\omega^2\bar{D}_3(x)\bar{\varphi}=0,$$
$$\frac{d^2\bar{w}}{dx^2}+\bar{G}_1(x)\frac{d\bar{w}}{dx}-\frac{d\bar{\varphi}}{dx}-\bar{G}_1(x)\bar{\varphi}+\omega^2\bar{G}_2(x)\bar{w}=0, \tag{10}$$

where the variable coefficients are defined as $\bar{D}_1(x)=\frac{D_{11}'(x)}{D_{11}(x)}$, $\bar{D}_2(x)=\frac{A_{55}(x)}{D_{11}(x)}$, $\bar{D}_3(x)=\frac{I_2(x)}{D_{11}(x)}$, $\bar{G}_1(x)=\frac{A_{55}'(x)}{A_{55}(x)}$, $\bar{G}_2(x)=\frac{I_0(x)}{A_{55}(x)}$. Here, and in what follows, the prime denotes differentiation with respect to the x-coordinate.

Preprints.org (www.preprints.org) | NOT PEER-REVIEWED | Posted: 12 July 2024 doi:10.20944/preprints202407.0993.v1

Hence, the solution of (10) at a specific point x_0 within the interval $0 \le x \le L$ in the domain of differential transformation is expressed by the recurrent algebraic equations:

$$\begin{aligned}\Phi(k+2) &= k_*\left\{-\sum_{p=0}^{k}(p+1)\Phi(p+1)D_1(k-p)+\sum_{p=0}^{k}\Phi(p)D_2(k-p)\right.\\ &\qquad\left.-\sum_{p=0}^{k}(p+1)W(p+1)D_2(k-p)-\omega^2\sum_{p=0}^{k}\Phi(p)D_3(k-p)\right\}\\ W(k+2) &= k_*\left\{-\sum_{p=0}^{k}(p+1)W(p+1)G_1(k-p)+\sum_{p=0}^{k}\Phi(p)G_1(k-p)\right.\\ &\qquad\left.+\sum_{p=0}^{k}(p+1)\Phi(p+1)L(k-p)-\omega^2\sum_{p=0}^{k}W(p)G_2(k-p)\right\}\end{aligned} \tag{11}$$

where $k_* = \frac{k!}{(k+2)!}$, $L(k)$ is a unity image, and $W(k)$, $\Phi(k)$, $D_1(k)$, $D_2(k)$, $D_3(k)$, $G_1(k)$, and $G_2(k)$ are the images of the unknown amplitudes $\bar{w}(x)$ and $\bar{\varphi}(x)$ and the corresponding functional coefficients in (10), respectively.

By incrementing the index k sequentially, we can generate all images from (11) except for $W(0)$, $W(1)$, $\Phi(0)$, and $\Phi(1)$. Consequently, the system (11) can be simplified to the form:

$$\begin{aligned}\Phi(k+2) &= B_\varphi(k)W(0)+C_\varphi(k)\Phi(0)+G_\varphi(k)W(1)+H_\varphi(k)\Phi(1),\\ W(k+2) &= B_w(k)W(0)+C_w(k)\Phi(0)+G_w(k)W(1)+H_w(k)\Phi(1)\end{aligned} \tag{12}$$

where the explicit forms of the recurrent coefficients in (12) are presented in [44] (see Appendix B).

Given that the images $W(k)$ and $\Phi(k)$ at $k \ge 2$ depend on $W(0)$, $W(1)$, $\Phi(0)$ and $\Phi(1)$, the original functions $\bar{w}(x)$ and $\bar{\varphi}(x)$ can be reconstructed for a selected number of images N as follows:

$$\begin{aligned}\bar{w}(x,\omega) &= \left\{1+\sum_{p=0}^{N-2}B_w(p)(x-x_0)^{p+2}\right\}W(0)+\left\{\sum_{p=0}^{N-2}C_w(p)(x-x_0)^{p+2}\right\}\Phi(0)\\ &\quad+\left\{(x-x_0)+\sum_{p=0}^{N-2}G_w(p)(x-x_0)^{p+2}\right\}W(1)+\left\{\sum_{p=0}^{N-2}H_w(p)(x-x_0)^{p+2}\right\}\Phi(1),\\ \bar{\varphi}(x,\omega) &= \left\{\sum_{p=0}^{N-2}B_\varphi(p)(x-x_0)^{p+2}\right\}W(0)+\left\{1+\sum_{p=0}^{N-2}C_\varphi(p)(x-x_0)^{p+2}\right\}\Phi(0)\\ &\quad+\left\{\sum_{p=0}^{N-2}G_\varphi(p)(x-x_0)^{p+2}\right\}W(1)+\left\{(x-x_0)+\sum_{p=0}^{N-2}H_\varphi(p)(x-x_0)^{p+2}\right\}\Phi(1).\end{aligned} \tag{13}$$

Taking into account the actual boundary conditions applied to the beam ends, which involve the transverse displacement $\bar{w}$, rotation angle $\bar{\varphi}$, bending moment $\bar{M}$, and shear force $\bar{Q}$, such that

$$\bar{M} = D_{11}(x)\frac{d\bar{\varphi}}{dx},\ \bar{Q} = A_{55}(x)\left(\frac{d\bar{w}}{dx}-\bar{\varphi}\right)$$

we can formulate the eigenvalue problem for each case of constraints in the form:

$$\begin{bmatrix}A_{11}(\omega) & A_{12}(\omega) & A_{13}(\omega) & A_{14}(\omega)\\ A_{21}(\omega) & A_{22}(\omega) & A_{23}(\omega) & A_{24}(\omega\\ A_{31}(\omega) & A_{32}(\omega) & A_{33}(\omega) & A_{34}(\omega\\ A_{41}(\omega) & A_{42}(\omega) & A_{43}(\omega) & A_{44}(\omega\end{bmatrix}\begin{pmatrix}W(0)\\ \Phi(0)\\ W(1)\\ \Phi(1)\end{pmatrix} = 0. \tag{14}$$

Here, the functions $A_{ij}(\omega)$ are appropriate polynomials of the unknown angular frequency ω, which involve the recurrent coefficients and the power terms of $(x - x_0)$.

Finally, the eigenvalues are computed by solving the root-finding problem resulting from the equation:

$$\det\left|A_{ij}(\omega)\right| = 0. \tag{15}$$

Preprints.org (www.preprints.org) | NOT PEER-REVIEWED | Posted: 12 July 2024 doi:10.20944/preprints202407.0993.v1

A computational program has been developed in the Matlab environment to apply the DTM for analyzing the free vibration of curvilinear tapered inhomogeneous Timoshenko beams. The eigenvalue problem is addressed using standard algorithms provided in the Matlab package [45].

3.2. Finite Element Modeling

To ensure the accuracy and validation of the proposed semi-analytical methodology for analyzing the free vibration parameters of curvilinearly tapered AFGM beams, a finite element model has been developed and utilized for comparison purposes. It is well-known that the optimal modeling strategy involves using graded finite elements (GFEs), which allow for the variation of material properties at the element level. Additionally, advanced three-dimensional models are essential to precisely capture the non-uniform geometry of axially inhomogeneous beams [31].

The free vibration analysis of AFGM beams is conducted using ABAQUS [46], incorporating a user-defined material subroutine (UMAT) to implement material gradients into a convenient three-dimensional element, C3D20, as detailed in [31,33] and illustrated in Figure 2b. The material gradient is assigned within the element volume during the computation of the element stiffness matrix, $\boldsymbol{K}^e$ using Gauss quadrature, as follows:

$$\boldsymbol{K}^e = \sum_{p=1}^{n_p}\sum_{q=1}^{n_q}\sum_{r=1}^{n_r}(\boldsymbol{B}^T\boldsymbol{D}(x)\boldsymbol{B}|\boldsymbol{J}|)_{p,q,r}w_p w_q w_r\,, \tag{16}$$

where the indices p, q, and r refer to the integration points over the element volume, $|\boldsymbol{J}|$ is the determinant of the geometric Jacobian matrix, w_p, w_q, and w_r are the Gaussian weights; $\boldsymbol{B}$ stands for a matrix of gradients of the shape functions for the 3-D element and the material matrix $\boldsymbol{D}(x)$ of the 3-D GFE relevant to this study can be found in [33].

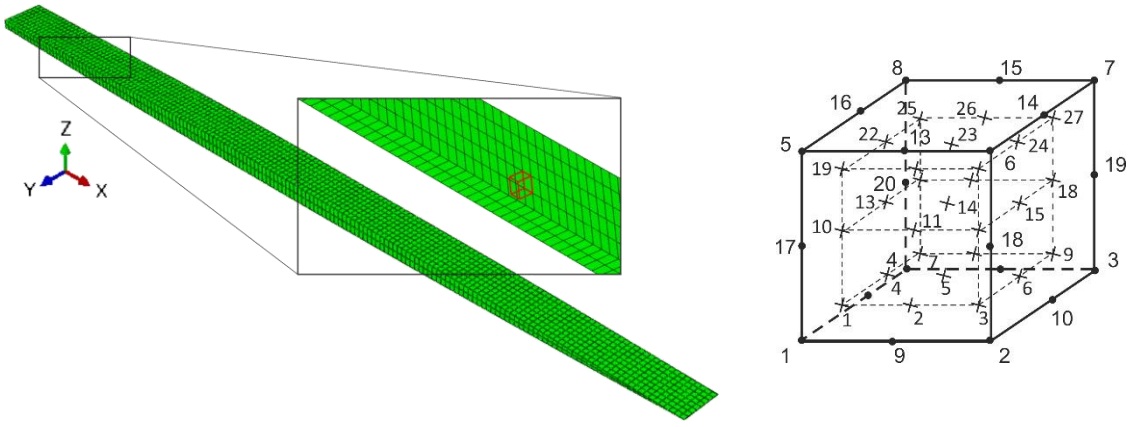

(**a**) (**b**)

Figure 2. Finite element model of the curvilinear tapered beam: (**a**) Finite element discretization with 3-D finite elements; (**b**) 20-node three-dimensional element C3D20 with a 3×3×3 point integration scheme.

ABAQUS currently does not support calculating the mass matrix based on a user-defined mass density in frequency analysis [46]. The elements available in ABAQUS use a constant mass density, i.e.

$$\boldsymbol{M}^e = \int_{V^e}\rho_0\boldsymbol{N}^T\cdot\boldsymbol{N}\,dV^e, \tag{17}$$

where $\boldsymbol{N}$ is an element interpolation matrix.

To address this limitation, we assigned a constant effective mass density within the GFE by using an average value of the actual mass density distribution over the beam's volume in the form:

$$\rho_{avr} = \frac{1}{V}\int_V \rho(x)\,dx \tag{18}$$

In the case of the free vibration analysis without damping, the global discrete system of governing equations of motion is reduced to the problem of eigenvalues and associated eigenvectors, which is written as follows

 doi:10.20944/preprints202407.0993.v1

$$(\boldsymbol{K} - \omega^2 \boldsymbol{M})\mathbf{X} = 0, \tag{19}$$

where $\boldsymbol{M}$, $\boldsymbol{K}$ are global mass and stiffness matrices, obtained by assembling the formulated element mass and stiffness matrices; ω is the undamped circular frequency, $\mathbf{X}$ is the vector of nodal displacements associated with oscillations at each ω. The free vibration analysis is carried out using linear perturbation load step, obtaining the eigenvalues by means of Lanczos or subspace iteration methods [46]. Figure 2a illustrates a 3-D finite element beam model created using the ABAQUS pre-processor, utilizing the 'loft' feature. To provide accurate results, the element aspect ratio in the mesh was consistently maintained close to one throughout all subsequent calculations.

4. Results

We will now examine beams with various curvilinear tapers in rectangular cross-sections, incorporating three distinct material variations along the beam axis. This analysis aims to demonstrate the effectiveness of the proposed computational technique by comparing the results with those obtained from other methods. First, we validate the accuracy of the DTM approach by benchmarking our findings against known solutions for uniform homogeneous and inhomogeneous Timoshenko beams under various boundary conditions. Then, we present a selection of examples for curvilinear taper beams, including both known and previously unexplored cases, to further illustrate the method's applicability and provide new insights that may be valuable to other researchers in this field.

4.1. Homogeneous Timoshenko Beams with Uniform Cross-Sections

The accuracy and effectiveness of the proposed approach are first benchmarked by computing the frequencies of homogeneous beams with uniform cross-sections.

We consider geometrically uniform ($w_1 = 0$) homogeneous ($m = n = 0$ with unit coefficients in (2)) beams with clamped-clamped (C-C), clamped-free (C-F), and simply supported (S-S) boundary conditions. The material and geometric parameters of the beams are listed in Table 1.

Table 1. The parameters of uniform beams.

L, m	b, m	h, m	E, Pa	G, Pa	ν	κ	ρ, kg/m³
1	0.02	0.1	2.1×10^{11}	0.875×10^{11}	0.2	0.845	7860

The first seven natural frequencies of the S-S, C-C, and C-F beams compared with those computed using the dynamic stiffness matrix method (DSM) in conjunction with the Timoshenko beam theory in [47] are presented in Table 2.

Table 2. The natural frequencies of uniform S-S, C-C, and C-F homogeneous beams based on different methods (Hz).

Mode number	S-S			C-C			C-F		
	DTM	[47]	Δ*, %	DTM	[47]	Δ, %	DTM	[47]	Δ, %
1	230.788	230.789	6.85E-5	500.587	0.58703	60E-6	82.8857	82.8860	2.82E-5
2	884.469	1884.469	01.29E-5	1288.763	1288.763	1.71E-5	498.191	1498.191	02.90E-5
3	1870.358	1870.358	1.43E-5	2339.160	2339.160	7.51E-6	1315.041	1315.041	1.36E-5
4	3091.056	3091.056	4.39E-6	3565.013	3565.013	9.38E-6	2394.776	2394.776	7.00E-6
5	4468.225	4468.225	9.51E-6	4910.439	4910.438	2.31E-5	3658.662	3658.662	5.88E-6
6	5946.852	5946.679	2.90E-3	6338.321	6337.691	9.94E-3	5044.291	5044.277	2.85E-3
7	7472.753	7489.650	2.26 E-1	7822.471	7821.911	7.16E-3	6508.492	6509.954	2.25E-2

* $\Delta = \frac{|\omega_{DSM} - \omega_{DTM}|}{\omega_{DSM}} \times 100\%$.

As shown in Table 2, there is excellent agreement between the solutions obtained using the DTM and DSM methods for all vibrational modes.

 doi:10.20944/preprints202407.0993.v1

4.2. Inhomogeneous Timoshenko beams with uniform cross-sections

Next, the ability of the proposed approach to accurately predict the frequencies of beams with uniform cross-sections made of inhomogeneous materials is evaluated.

We assume that the beam's mass density and modulus of elasticity follow power-law distributions of *Type 1* as described in (2). Since natural frequencies for Timoshenko beams under these conditions are not documented in the literature, we will compare our results with those obtained using the Euler-Bernoulli beam theory in [14] for AFGM beams with a slenderness ratio of $L/h = 50$. The geometrical and material parameters are consistent with those detailed in [14] (see Tables 4–6 and Appendix B).

The comparison of the first five dimensionless frequencies $\bar{\omega} = \omega L^2 \sqrt{\frac{\rho_0 A}{E_0 J}}$ for the cantilever AFGM beam is presented in Table 3. Furthermore, to extend this study to beams, where shear deformation plays a significant role, we also provide in Table 3 the natural frequencies computed for beams with a slenderness ratio of 10.

Table 3. Dimensionless natural frequencies of uniform cantilever AFGM beams.

n \ m	0				1				2			
	[14]	**DTM**	**Δ**, %**	**DTM***	**[14]**	**DTM**	**Δ, %**	**DTM***	**[14]**	**DTM**	**Δ, %**	**DTM***
	17.92823	17.9268	7.98E-3	17.7871921.05590	21.0543		7.59E-3	20.8983724.2944824.29265			7.53E-3	24.11362
	112.3543	112.2918	5.56E-2	106.6048140.9285	140.8521		5.43E-2	133.8822162.7971	162.7083		5.46E-2	154.6099
0	314.5953	314.1788	1.33E-1	280.3868403.4795	402.9577		1.30E-1	360.512 462.7162	462.1126		1.31E-1	413.0607
	616.4812	614.9754	2.45E-1	508.6127795.2794	793.3707		2.41E-1	658.1122909.6774	907.4782		2.42E-1	751.8375
	1019.088	1015.124	3.90E-1	774.24711317.8941	312.838		3.85E-1	1004.3561505.5841	499.772		3.87E-1	1145.767
	18.89966	18.89824	7.52E-3	18.7592122.2986	722.29709		7.10E-3	22.1424125.7371	325.73531		7.07E-3	25.55769
	124.9620	124.8901	5.76E-2	118.3494158.3713	158.2830		5.58E-2	150.2293182.9067	182.8039		5.63E-2	173.4348
1	355.0148	354.5324	1.36E-1	315.5107460.6318	460.0258		1.32E-1	410.8001527.8895	527.1870		1.33E-1	470.1954
	698.2161	696.4732	2.50E-1	573.9377911.2419	909.0284		2.44E-1	752.45011041.6331	039.076		2.46E-1	858.5914
	1155.920	1151.340	3.98E-1	874.67081512.2571	506.403		3.89E-1	1150.0921726.5721	719.828		3.92E-1	1310.355
	18.99432	18.99291	7.43E-3	18.8547322.4553	122.45374		6.98E-3	22.3005 25.9212	325.91943		6.96E-3	25.74348
	127.1780	127.1041	5.82E-2	120.3839162.3684	162.2768		5.64E-2	153.9285187.5542	187.4475		5.69E-2	177.7289
2	363.0379	362.5411	1.37E-1	322.3891475.3808	474.7514		1.33E-1	423.6509544.8226	544.0922		1.34E-1	484.8789
	714.8085	713.0133	2.52E-1	586.9809941.7464	939.4477		2.45E-1	776.99211076.5971	073.939		2.47E-1	886.5256
	1183.930	1179.213	4.00E-1	894.84161563.7281	557.652		3.90E-1	1188.2311785.5351	778.528		3.94E-1	1353.679
	18.97105	18.96963	7.50E-3	18.8309922.4520	222.45045		6.99E-3	22.2971525.9188	425.91704		6.94E-3	25.74104
	126.3443	126.2712	5.79E-2	119.6185162.2392	162.1477		5.64E-2	153.8091187.4615	187.3548		5.69E-2	177.6432
3	359.5311	359.0406	1.37E-1	319.3864474.8301	474.2016		1.33E-1	423.1715544.4325	543.7027		1.34E-1	484.5410
	707.2811	705.5100	2.51E-1	581.0888940.5708	938.2755		2.45E-1	776.04931075.7651	073.110		2.47E-1	885.8633
	1171.009	1166.357	3.99E-1	885.59521561.7171	555.650		3.90E-1	1186.7471784.1131	777.111		3.94E-1	1352.638
	18.97367	18.97225	7.46E-3	18.8336922.4493	322.44776		7.01E-3	22.2943725.92410	25.9223		6.94E-3	25.74647
	126.4718	126.3986	5.80E-2	119.7366162.0943	162.0029		5.64E-2	153.6739187.7400	187.6332		5.69E-2	177.9022
4	360.1566	359.6650	1.37E-1	319.9237474.1105	473.4831		1.33E-1	422.5427545.7931	545.0612		1.34E-1	485.7226
	708.6890	706.9135	2.51E-1	582.1911938.9675	936.6766		2.45E-1	774.76181078.7911	076.127		2.48E-1	888.2724
	1173.481	1168.816	3.99E-1	887.36171558.9181	552.864		3.90E-1	1184.6831789.3891	782.364		3.94E-1	1356.492
	-	-	-	-	22.4499	422.44838	6.97E-3	22.2950125.9227	425.92094		6.93E-3	25.74504
5	-	-	-	-	162.1362	162.0448	5.64E-2	153.7134187.6486	187.5419		5.69E-2	177.8163
	-	-	-	-	474.3503	473.7225	1.33E-1	422.7534545.2794	544.5482		1.34E-1	485.2744

 doi:10.20944/preprints202407.0993.v1

	-	-	-	-	939.5286	937.2362	2.45E-1	775.2134	1077.591	1074.931	2.48E-1	887.3160
	-	-	-	-	1559.921	1553.862	3.90E-1	1185.423	1787.249	1780.233	3.94E-01	1354.929
	-	-	-	-	-	-	-	-	25.9229	625.92116	6.96E-3	25.74528
	-	-	-	-	-	-	-	-	187.6670	187.5602	5.69E-2	177.8338
6	-	-	-	-	-	-	-	-	545.3964	544.6650	1.34E-1	485.3772
	-	-	-	-	-	-	-	-	1077.880	1075.218	2.48E-1	887.5466
	-	-	-	-	-	-	-	-	1787.776	1780.758	3.94E-1	1355.315

* Dimensionless frequencies of the cantilever AFGM beam with $L/h = 10$; ** $\Delta = \frac{|\omega_{Ref} - \omega_{DTM}|}{\omega_{Ref}} \times 100\%$.

Upon reviewing Table 3, it becomes evident that both Euler-Bernoulli and Timoshenko beams with slenderness ratio of 50 demonstrate excellent agreement for the fundamental frequency and show slight deviations for higher frequencies. This is because the Euler-Bernoulli beam theory overestimates especially higher frequencies due to its neglect of shear effect. Specifically, when the slenderness ratio is 10, the fundamental frequencies of the beams show only satisfactory matching, while significant discrepancies are observed in higher-order frequencies, consistent with theoretical expectations.

In the second example, we evaluate the accuracy of predicted natural frequencies for exponential AFGM beams. The current results are compared with those obtained in [11] using the Chebyshev collocation method. The beams are composed of zirconia and aluminum with axial gradation according to law (4), where the ceramic volume fraction is an exponential function: $V_c = \frac{e^{\alpha x/L} - 1}{e^{\alpha} - 1}$. The material and geometrical properties of the beams are described in [11] and detailed in Table 4 as follows:

Table 4. The parameters of uniform exponential-law AFGM beams.

L, m	b, m	h, m	E, GPa		ρ, kg/m³		ν
			ZrO_2	Al	ZrO_2	Al	
1	0.01	0.03	200	70	3800	2702	0.3

The computed first four dimensionless natural frequencies $\bar{\omega} = \omega L^2 \sqrt{\frac{\rho_{Al} A}{E_{Al} J}}$ of the exponential-law AFGM beams under S-S and C-C boundary conditions for various exponents α compared with the results in [11] are given in Table 5.

Table 5. Dimensionless natural frequencies of uniform exponential-law AFGM beams.

BCs	α	-10			-3			0			3			10		
	Mode	[11]	DTM	Δ*, %	[11]	DTM	Δ, %	[11]	DTM	Δ, %	[11]	DTM	Δ, %	[11]	DTM	Δ, %
S-S	1	9.9225	9.8357	0.88	10.351	10.351	4.8E-4	10.849	10.849	3.7E-4	11.225	11.225	6.2E-4	11.437	11.447	9.2E-2
	2	39.834	39.363	1.18	41.716	41.716	2.4E-5	43.396	43.396	6.9E-5	44.571	44.571	4.9E-4	45.394	45.446	1.2E-1
	3	89.325	89.576	0.28	93.239	93.239	2.2E-5	96.793	96.793	3.1E-5	99.431	99.431	1.7E-4	101.21	101.31	9.2E-2
	4	157.50	156.01	0.94	164.07	164.07	6.1E-6	170.22	170.22	2.4E-5	174.87	174.87	3.0E-4	177.98	178.17	1.1E-1
C-C	1	24.646	24.613	0.14	24.780	24.780	1.6E-4	24.223	24.223	1.2E-4	23.794	23.794	7.6E-4	23.907	23.925	7.5E-2
	2	65.291	65.232	0.09	66.155	66.155	1.5E-5	66.621	66.621	4.5E-5	66.780	66.781	1.2E-3	67.120	67.176	8.3E-2
	3	124.53	123.97	0.44	127.04	127.04	1.6E-5	129.55	129.55	7.7E-6	131.09	131.09	7.5E-4	131.94	132.03	6.8E-2
	4	201.23	201.32	0.05	206.29	206.29	1.6E-4	211.61	211.61	1.9E-5	215.14	215.15	1.7E-3	216.92	217.10	8.3E-2

* $\Delta = \frac{|\omega_{Ref} - \omega_{DTM}|}{\omega_{Ref}} \times 100\%$.

From Table 5, it is obvious that the present results for all first four frequencies closely align with those obtained in the referenced study.

Preprints.org (www.preprints.org) | NOT PEER-REVIEWED | Posted: 12 July 2024 doi:10.20944/preprints202407.0993.v1

Finally, uniform aluminum-zirconia Timoshenko beams with axial variation of the material characteristics according to the power-law function $V_c = \left(\frac{x}{L}\right)^{\beta}$ of the ceramic volume fraction in the rule of mixtures (4) are tested. The natural frequencies of these beams are benchmarked against the findings in [15]. The parameters of the AFGM beams are the same as those in [15] and are listed in Table 4.

The first four dimensionless natural frequencies $\bar{\omega} = \omega L^2 \sqrt{\frac{\rho_{ZrA}}{E_{ZrJ}}}$ of the AFGM beams under C-F, S-S and C-C boundary conditions for various indices β, compared with the solutions obtained using the differential quadrature element method in [15], are shown in Table 6.

Inspecting Table 6 reveals excellent agreement between the first four frequencies obtained in this study and those reported in the referenced research across all boundary conditions and power indices.

Table 6. Dimensionless natural frequencies of uniform power-law AFGM beams.

BCs	β	1			2			3		
	Mode	[15]	DTM	Δ*, %	[15]	DTM	Δ, %	[15]	DTM	Δ, %
C-F	1	3.89630	3.896310	2.57E-4	3.88280	3.883120	8.24E-3	3.79570	3.797640	5.37E-2
	2	15.0505	15.05049	5.98E-4	15.2590	15.25982	6.03E-3	15.2936	15.30040	4.51E-2
	3	30.9409	30.94087	1.20E-3	31.6180	31.61871	3.19E-3	31.9962	32.00717	3.55E-2
	4	46.3782	46.37814	1.16E-3	47.6349	47.63506	1.60E-3	48.3335	48.34427	2.37E-2
S-S	1	7.84590	7.845920	2.55E-4	7.98730	7.988010	1.01E-2	8.06450	8.069630	6.49E-2
	2	23.9406	23.94060	8.35E-4	24.2521	24.25241	2.10E-3	24.3532	24.35745	1.87E-2
	3	41.6789	41.67887	1.37E-3	42.3024	42.30265	2.01E-3	42.5010	42.50566	1.24E-2
	4	53.7111	53.71108	2.01E-3	54.8771	54.87722	2.22E-3	55.3881	55.38793	1.68E-3
C-C	1	12.9065	12.90653	1.01E-3	12.6873	12.68758	3.78E-3	12.6030	12.60572	2.32E-2
	2	26.7597	26.75967	1.38E-3	26.6416	26.64177	1.76E-3	26.5809	26.58381	1.21E-2
	3	43.0417	43.04166	1.53E-3	43.3694	43.36938	1.34E-3	43.4958	43.49723	4.67E-3
	4	58.5205	58.52006	7.86E-4	59.2779	59.27826	1.96E-3	59.5726	59.57154	2.69E-4

* $\Delta = \frac{|\omega_{Ref} - \omega_{DTM}|}{\omega_{Ref}} \times 100\%$.

It should be noted that throughout this series of examples, the proposed approach demonstrates high accuracy, efficiency, and rapid convergence. Only thirty terms in the series expansions (13) are sufficient to yield accurate results for the first several natural frequencies.

4.3. Homogeneous Timoshenko Beams with Curvilinearly Tapered Cross-Sections

In order to demonstrate the applicability and effectiveness of the DTM in solving the free vibration problem for axially curvilinear cross-sectional beams, we now consider various specific cases. Whenever possible, we compare the results obtained using DTM with those already documented in the literature. In cases, where comparative data is not available, we perform the frequency analysis using ABAQUS software.

The first problem addressed is a homogeneous beam with a double-parabolic taper, truncated at the left end. The shape of the parabolic taper beam is analytically defined by the weight $w_1 = 1$, the parameter l_e equals to the truncation factor δ_0 and the tringle $\boldsymbol{P}_0\boldsymbol{P}_1\boldsymbol{P}_2$ specified as shown in Figure 3a.

Preprints.org (www.preprints.org) | NOT PEER-REVIEWED | Posted: 12 July 2024 doi:10.20944/preprints202407.0993.v1

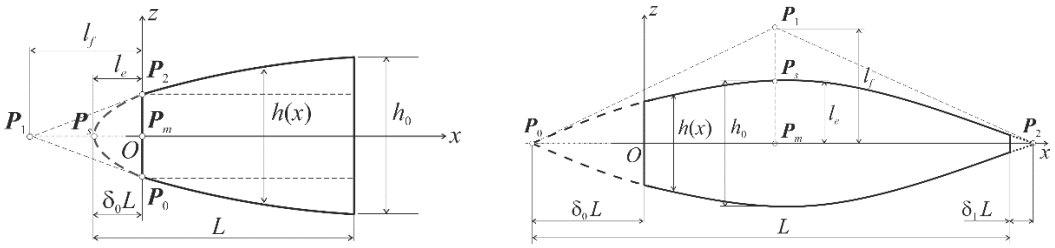

Figure 3. The geometries of double-parabolic taper beams truncated at the left end: (a) Parabola branches directed to the right; (b) Parabola branches directed to downward.

Due to the lack of data for such Timoshenko beams in the published literature, the results are compared with those obtained using the Rayleigh-Ritz method within the Euler-Bernoulli beam theory in [2]. Table 7 presents the first three dimensionless frequencies $\bar{\omega} = \omega(L-\delta_0)^2\sqrt{\frac{\rho A_0}{EJ_0}}$ for both the reference Euler-Bernoulli and present Timoshenko beams with a slenderness ratio $L/h_0 = 50$ under three different boundary conditions and different truncation factors.

Table 7. Dimensionless natural frequencies of homogeneous beams with double-parabolic taper.

δ_0	BCs	C-C			S-S			F-C		
	Mode	[2]	DTM	Δ*, %	[2]	DTM	Δ, %	[2]	DTM	Δ, %
0.1	1	14.368	14.35795	0.07	6.3778	6.379480	0.03	5.3883	5.371650	0.31
	2	40.479	40.36953	0.27	27.310	27.28302	0.10	20.699	20.55328	0.70
	3	80.211	79.77238	0.55	61.023	60.84181	0.30	48.471	47.93399	1.11
0.2	1	15.972	15.9348	0.23	7.0594	7.054580	0.07	4.8654	4.862540	0.06
	2	44.578	44.3374	0.54	29.395	29.32546	0.24	20.372	20.32497	0.23
	3	87.897	87.0621	0.95	65.800	65.45681	0.52	49.870	49.61366	0.51
0.3	1	17.176	17.11698	0.34	7.5823	7.575210	0.09	4.5179	4.514900	0.07
	2	47.701	47.32308	0.79	31.082	30.97545	0.34	20.420	20.35704	0.31
	3	93.828	92.52728	1.39	69.692	69.16329	0.76	51.543	51.17858	0.71
0.4	1	18.175	18.08114	0.52	8.0198	8.008940	0.14	4.2660	4.262320	0.09
	2	50.325	49.73045	1.18	32.561	32.39500	0.51	20.592	20.50043	0.44
	3	98.855	96.82087	2.06	73.098	72.27499	1.13	53.199	52.65124	1.03
0.5	1	19.044	18.89066	0.81	8.4018	8.384520	0.21	4.0729	4.067820	0.12
	2	52.633	51.66934	1.83	33.904	33.63600	0.79	20.812	20.67111	0.68
	3	103.30	100.0365	3.16	76.179	74.85468	1.74	54.785	53.92227	1.57
0.6	1	19.852	19.55547	1.49	8.7443	8.71463	0.34	3.9188	3.9112	0.19
	2	54.718	53.06449	3.02	35.148	34.68662	1.31	21.052	20.81738	1.11
	3	107.34	101.82207	5.14	79.021	76.76144	2.86	56.296	54.84588	2.58
0.7	1	20.531	20.01665	2.51	9.0569	8.99939	0.63	3.7922	3.77915	0.34
	2	56.634	53.51562	5.51	36.315	35.43022	2.44	21.299	20.85956	2.06
	3	111.06	96.84761	12.80	81.676	77.40895	5.22	57.736	55.03705	4.67
0.8	1	21.186	19.98305	5.68	9.3459	9.207100	1.49	3.6859	3.493240	5.23
	2	58.417	43.48449	25.6	37.419	35.37001	5.48	21.547	19.53236	9.35
	3	114.54	69.00506	39.8	84.180	51.02468	39.4	59.112	63.26979	7.03

* $\Delta = \frac{|\omega_{Ref}-\omega_{DTM}|}{\omega_{Ref}} \times 100\%$.

Preprints.org (www.preprints.org) | NOT PEER-REVIEWED | Posted: 12 July 2024 doi:10.20944/preprints202407.0993.v1

One can observe from Table 7 that the eigenfrequencies closely match for both types of beams when the truncation factor is small. However, as the truncation factor increases, discrepancies between them become more pronounced, especially for the third mode. This difference is anticipated because shorter beams necessitate accounting for shear deformation, which the simpler Euler-Bernoulli beam model does not address.

The second benchmark example involves a beam with a parabolic-tapered height and constant width, truncated at the left end and tapered to a point at the right end ($\delta_1 = 0$), as illustrated in Figure 3b. A detailed specification of this beam configuration is provided in [3]. The analytical presentation of this shape of the parabolic beam with Bézier curves is discussed in Section 2.1.

Once again, due to limited availability of data for Timoshenko beams in the existing literature, comparisons are made with results obtained using hypergeometric functions within the framework of the Euler-Bernoulli beam theory, as described in [3]. Table 8 displays the first four dimensionless frequencies $\bar{\omega} = \omega(L/2)^2\sqrt{\frac{\rho A_0}{EJ_0}}$ of cantilever Euler-Bernoulli and Timoshenko beams with a slenderness ratio $L/h_0 = 50$ for various truncation factors.

Table 8. Dimensionless natural frequencies of cantilever homogeneous beams with parabolic taper height and constant width.

δ_0	0.15			0.2			0.25			0.3			0.35		
Mode	**[3]**	**DTM**	**Δ*, %**	**[3]**	**DTM**	**Δ, %**	**[3]**	**DTM**	**Δ, %**	**[3]**	**DTM**	**Δ, %**	**[3]**	**DTM**	**Δ, %**
1	1.050	1.05057	0.05	1.469	1.46748	0.10	1.936	1.93539	0.03	2.465	2.46322	0.07	3.070	3.06690	0.10
2	7.606	7.58803	0.24	8.958	8.93699	0.23	10.42	10.3849	0.34	12.02	11.9846	0.29	13.83	13.7831	0.34
3	18.25	18.2256	0.13	20.91	20.8092	0.48	23.79	23.6579	0.56	26.96	26.7977	0.60	30.54	30.3304	0.69
4	32.54	31.9653	1.77	36.96	36.6841	0.75	41.73	41.3659	0.87	46.99	46.5406	0.96	52.92	52.3541	1.07
δ	**0.4**			**0.45**			**0.5**			**0.55**			**0.6**		
1	3.770	3.76591	0.11	4.593	4.58701	0.13	5.576	5.56729	0.16	6.772	6.76070	0.17	8.263	8.24726	0.19
2	15.91	15.8416	0.43	18.32	18.2384	0.45	21.18	21.0814	0.47	24.65	24.5248	0.51	28.96	28.7980	0.56
3	34.63	34.3716	0.75	39.40	39.0763	0.82	45.05	44.6586	0.87	51.9	51.4115	0.94	60.41	59.7941	1.02
4	59.70	59.0060	1.16	67.61	66.7478	1.28	76.98	75.9204	1.38	88.34	87.0392	1.47	102.4	100.825	1.54
δ	**0.65**			**0.7**			**0.75**			**0.8**			**0.85**		
1	10.17	10.1532	0.16	12.72	12.6888	0.25	16.27	16.2322	0.23	21.60	21.5566	0.20	30.47	30.3768	0.31
2	34.47	34.2610	0.61	41.78	41.5124	0.64	51.99	51.6294	0.69	67.26	66.6661	0.88	92.66	91.9427	0.77
3	71.29	70.5089	1.10	85.72	84.7297	1.16	105.9	104.568	1.26	136.0	134.452	1.14	186.2	183.606	1.39
4	120.5	118.443	1.71	144.4	141.823	1.78	177.8	174.436	1.89	227.8	222.612	2.28	310.9	304.354	2.11

* $\Delta = \frac{|\omega_{Ref} - \omega_{DTM}|}{\omega_{Ref}} \times 100\%$.

From Table 8, one can see that the compared natural frequencies exhibit close agreement. Similar to the previous example, as the beam length decreases, discrepancies between the present and benchmarked results increase, especially for higher modes, due to the greater influence of shear deformation, as discussed earlier.

Therefore, these examples thoroughly confirm the reliability of the proposed computational method for analyzing curvilinear tapered beams.

4.4. AFGM Timoshenko Beams with Curvilinearly Tapered Cross-Sections

This subsection presents the performance of the DTM for frequency analysis of inhomogeneous curvilinearly tapered beams of convex-up and concave-down shapes, referred to as plump and slender models in [29], illustrated in Figure 1a,b, respectively. The material properties of the beams vary axially according to the laws specified in (3) for *Type 2* and (4) for *Type 3* distributions. Detailed geometric and material properties of the beams can be found in [29] and are summarized in Table 9.

 doi:10.20944/preprints202407.0993.v1

Table 9. The parameters of curvilinearly non-uniform AFGM beams.

Material	E, GPa	ρ, kg/m³	ν	L, m	b_0, m	h_0, m	l_e, m	l_f, m
Aluminum	70	2700	0.3					
Steel	348.43	2370	0.24	1	0.2	0.2	0.04	0.1
Si_3N_4	201.04	8166	0.33					

First, we analyze beams with varying thickness and constant width for both *Type 2* and *Type 3* material laws. The exponential law (3) with parameter $a = 1$ and gradient indices $\gamma_e = 0, 1, 5$ is applied to beams made of aluminum, whereas the power-law (4) with parameter $b = 1$ and gradient indices $\gamma_c = 0, 1, 5$ is utilized for beams composed of a combination of steel (SUS304) and ceramic (Si_3N_4) phases, as done in [29].

Table 10 presents the first two frequencies associated with the bending modes of the curvilinear taper beams with C-C boundary conditions. These frequencies are compared with those computed using NURBS in the 3-D finite element analysis conducted in [29].

Table 10. Natural frequencies, Hz, of the C-C AFGM beams with curvilinear taper height and constant width.

AFGM	Model	γ_e/γ_c	0			1			5		
		Mode	[29]	DTM	Δ*, %	[29]	DTM	Δ, %	[29]	DTM	Δ, %
Type 2	Plump	1	889.39	887.304	0.23	891.48	889.589	0.21	997.39	1002.94	0.56
		2	1889.1	2034.36	7.69	1894.4	2041.25	7.75	2025.3	2203.40	8.79
	Slender	1	800.93	779.141	2.72	805.63	783.893	2.70	920.25	899.469	2.26
		2	1774.6	1728.28	2.61	1778.8	1732.06	2.63	1882.4	1838.13	2.35
Type 3	Plump	1	2128.3	2133.71	0.25	1229.4	1226.23	0.26	947.74	947.074	0.07
		2	4532.2	4911.19	8.36	2632.4	2837.54	7.79	2036.2	2199.87	8.04
	Slender	1	1906.2	1865.29	2.15	1108.2	1078.24	2.70	851.24	828.860	2.63
		2	4239.8	4151.87	2.07	2471.8	2406.75	2.63	1902.5	1856.66	2.41

* $\Delta = \frac{|\omega_{Ref} - \omega_{DTM}|}{\omega_{Ref}} \times 100\%$.

The current results align satisfactory with the reference data, demonstrating differences of less than 0.6% for the fundamental frequency and less than 9% for the second frequency in the plump beams. For slender beams, the discrepancies are approximately 3% for both frequencies. These deviations arise from differences in modeling approaches. The current model uses a line beam structure with a first-order shear theory, whereas the IGA analysis in [29] employs a more detailed 3-D beam modeling approach.

Next, we analyze the parabolic convex beams depicted in Figure 3b. These beams feature a parabolic taper in height and maintain a constant width. They are truncated at the left end with a fixed factor $\delta_0 = 0.5$, while the right end is characterized by a variable truncation factor δ_1. The beam ends are subjected to C-C and C-F constraints. The material constants, given in Table 1, vary along the beam length according to the *Type 1* material law with a linear distribution for Young's modulus ($n = 1$) and a parabolic distribution for mass density ($m = 2$) as described in (2). Detailed specifications of these beam configurations are provided in [23].

While benchmark results for the fundamental frequencies of these beams are available in [23], higher-order frequencies are absent in the existing literature. Therefore, the results obtained using the DTM are validated against finite element analysis for these beams, as discussed in Section 3.2.

The comparison of first five dimensionless bending frequencies $\bar{\omega} = \omega L^2 \sqrt{\frac{\rho_0 A_0}{E_0 J_0}}$, depending on the truncation factor δ_1 for the two types of boundary conditions is shown in Table 11. It is observed that the differences between dimensionless fundamental frequencies obtained from the present analysis, published results and FEM predictions are quite small. However, the higher frequencies

Preprints.org (www.preprints.org) | NOT PEER-REVIEWED | Posted: 12 July 2024 doi:10.20944/preprints202407.0993.v1

show more significant deviations between the DTM and FEM solutions. Likely, these discrepancies between the two sets of data are attributed to methodological differences in formulation and solution approach. Overall, these findings confirm the reliability of the DTM approach within acceptable limits.

As mode shapes play a crucial role in evaluating the accuracy of structural dynamics modeling, the first five bending mode shapes associated with the appropriate frequencies of AFGM beams with $\delta_1 = 0.2$ for C-C and C-F boundary conditions, as listed in Table 11 and obtained using the DTM, are plotted in Figure 4a,b, respectively.

Table 11. Dimensionless natural frequencies of truncated AFGM beams with parabolic taper height and constant width.

BCs	δ_1	0.2				0.4				0.6			
	Mode	[23]	FEM	DTM	Δ*, %	[23]	FEM	DTM	Δ*, %	[23]	FEM	DTM	Δ*, %
C-C	1	18.4750	18.8461	18.5033	0.15	16.4231	6.7328	16.4583	0.21	14.1591	14.7828	14.2013	0.30
	2	-	53.7872	51.5889	4.09	-	47.1474	46.5676	1.23	-	42.3017	40.8931	3.33
	3	-	105.999	101.332	4.40	-	93.1729	92.1155	1.13	-	84.2618	81.5879	3.17
	4	-	175.772	167.090	4.94	-	154.114	152.461	1.07	-	139.905	135.640	3.05
	5	-	261.850	248.400	5.14	-	229.652	227.231	1.05	-	208.997	202.736	3.00
C-F	1	2.5715	2.7107	32.5711	5.01	2.7594	2.9488	52.7593	3.00	3.0151	3.1738	1.0.146	0.02
	2	-	18.8484	18.0533	4.22	-	18.3961	17.5276	4.72	-	18.0266	17.0113	5.63
	3	-	54.3519	51.7463	4.79	-	49.5819	48.3800	2.42	-	46.8092	44.6929	4.52
	4	-	107.161	101.628	5.16	-	95.5807	94.1178	1.53	-	88.8564	85.6122	3.65
	5	-	177.343	167.573	5.51	-	156.448	154.637	1.16	-	142.196	139.622	1.81

* $\Delta = \frac{|\omega_{Ref} - \omega_{DTM}|}{\omega_{Ref}} \times 100\%$.

Analogously, Figure 5a,b illustrate the bending mode shapes of the same truncated AFGM beams, constructed based on the FEM results, which are given in Table 11.

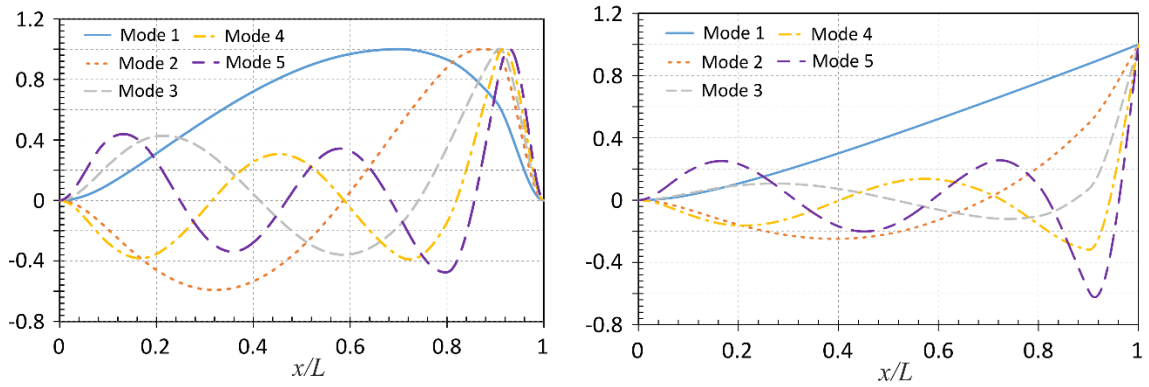

Figure 4. Mode shapes of truncated AFGM beams with parabolic taper height and constant width obtained from DTM analysis: (**a**) C-C boundary conditions; (**b**) C-F boundary conditions.

It is worth noticing that the geometric non-uniformity and the variation of material parameters along the beam length significantly affect the mode shapes. The figures clearly show that the positions of the nodal points shift along the beam length, and this shift is more pronounced as the truncation factor δ_1 becomes smaller.

 doi:10.20944/preprints202407.0993.v1

4.5. AFGM Timoshenko Beams with Curvilinearly Double-Tapered Cross-Sections

To the best of authors' knowledge, benchmark results for curvilinearly double-tapered AFGM beams are not available in the existing literature. Hence, the results of the present analysis are validated against axial plumb and slender beams with *Type 2* and *Type 3* material distributions, as considered in [29], which feature variable thickness and constant width. Further, the analysis will be etended to include beams with double-tapered cross-sectional variations. The geometrical and material parameters are identical to those used in the previous examples of curvilinear taper beams with exponential and power-law gradations as presented in [29].

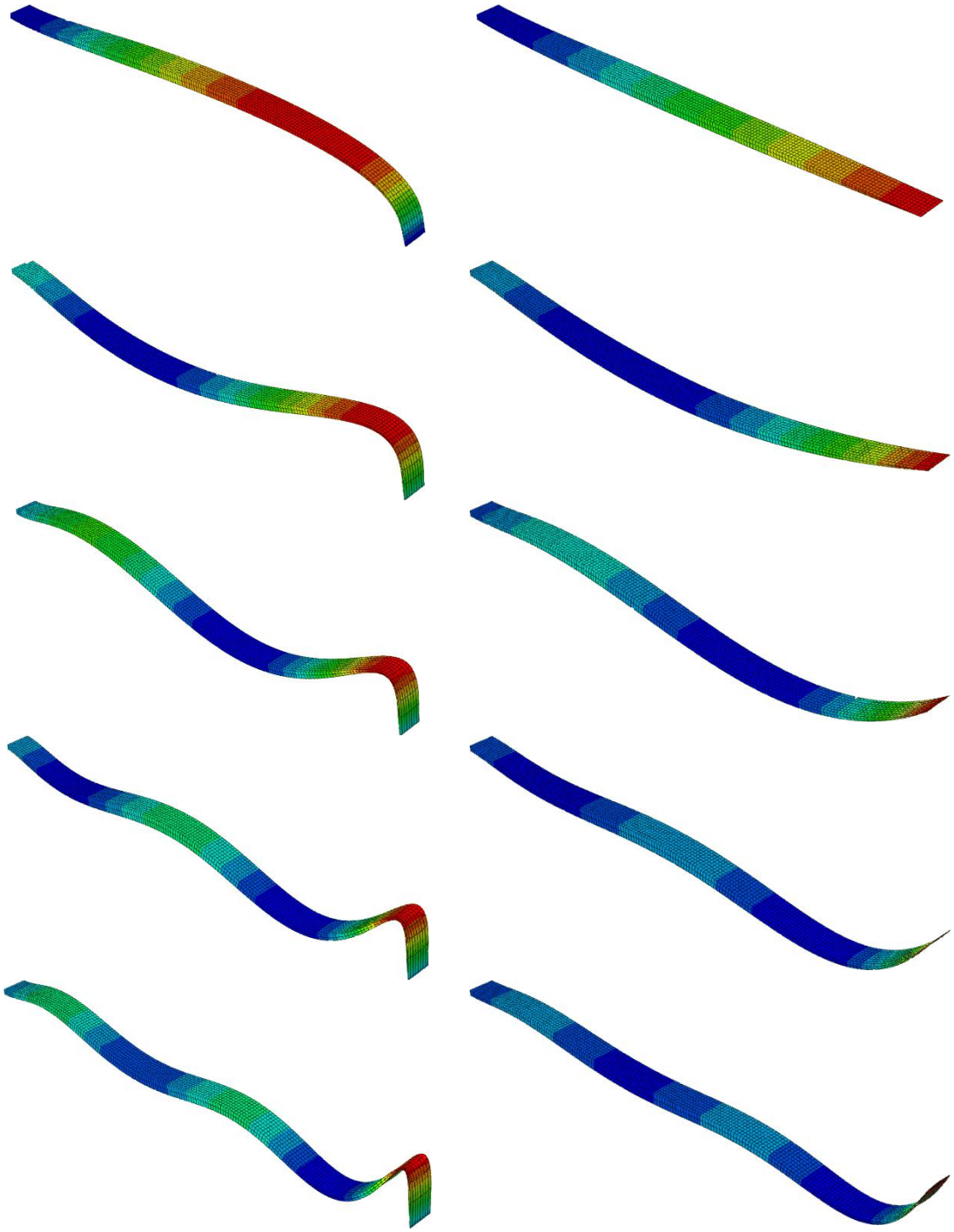

Figure 5. Mode shapes of truncated AFGM beams with parabolic taper height and constant width obtained from 3- D FEM analysis: (a) C-C boundary conditions; (b) C-F boundary conditions.

Preprints.org (www.preprints.org) | NOT PEER-REVIEWED | Posted: 12 July 2024 doi:10.20944/preprints202407.0993.v1

The first two dimensionless frequencies $\bar{\omega} = \omega L\sqrt{\frac{\rho_{Al}}{E_{Al}}}$ of axially graded *Type 2* plump and slender C-C beams with variable thickness and constant width, as well beams with simultaneously variable thickness and width, depending on the exponential law parameter a and gradient index γ_e are collected in Table 12. Satisfactory agreement between the reference and present results for plump and slender AFGM beams with variable thickness is observed. The errors between the frequencies fall within the range observed for frequencies of similar beams with $a = 1$ and $\gamma_e = 1$ in Table 10. In particular, minor deviations are noted for the first frequency, while higher discrepancies are observed for the second frequency.

Table 12. Dimensionless natural frequencies of curvilinear taper C-C AFGM beams with various exponential law (3) parameters.

Model	a	0.2			0.5			0.8			1.0		
	γ_e	[29]	DTM	DTM*	[29]	DTM	DTM*	[29]	DTM	DTM*	[29]	DTM	DTM*
Plump	0	1.0975	1.094931.03005		1.0975	1.094931.03005		1.0975	1.094931.03005		1.0975	1.094931.03005	
		2.3311	2.510392.41452		2.3311	2.510392.41452		2.3311	2.510392.41452		2.3311	2.510392.41452	
	0.5	1.0975	1.094951.03006		1.0977	1.095091.03012		1.0979	1.096691.03025		1.0981	1.095601.03037	
		2.3312	2.510472.41461		2.3316	2.510922.41510		2.3322	2.515832.41601		2.3328	2.512522.41685	
	1	1.0976	1.095031.03010		1.0981	1.095601.03037		1.0991	1.099231.03093		1.1001	1.097741.03149	
		2.3314	2.510732.41489		2.3328	2.512522.41685		2.3353	2.525592.42049		2.3377	2.518892.42384	
	2	1.0979	1.095361.03025		1.1001	1.097741.03149		1.1047	1.102741.03446		1.1095	1.107991.03796	
		2.3322	2.511752.41601		2.3377	2.518892.42384		2.348	2.532122.43829		2.3575	2.544292.45154	
	5	1.1001	1.097741.03149		1.1181	1.117331.04478		1.1689	1.171751.09083		1.2308	1.237631.15183	
		2.3377	2.518892.42384		2.3725	2.563242.47209		2.4379	2.6446	2.55945	2.4992	2.718982.63835	
Slen-der	0	0.9883	0.961451.06330		0.9883	0.961451.06330		0.9883	0.961451.06330		0.9883	0.961451.06330	
		2.1899	2.132692.27063		2.1899	2.132692.27063		2.1899	2.132692.27063		2.1899	2.132692.27063	
	0.5	0.9884	0.961511.06337		0.9887	0.962921.06368		0.9893	0.962391.06427		0.9898	0.962921.06482	
		2.1899	2.132732.27063		2.1902	2.133852.27066		2.1907	2.133432.27071		2.1912	2.133852.27076	
	1	0.9886	0.961691.06355		0.9898	0.962921.06482		0.9921	0.965211.06718		0.9941	0.967321.06936	
		2.1901	2.132872.27065		2.1912	2.133852.27076		2.1932	2.135672.27101		2.1951	2.137352.27128	
	2	0.9893	0.962391.06427		0.9941	0.967321.06936		1.0032	0.976481.07883		1.0116	0.984961.08759	
		2.1907	2.133432.27071		2.1951	2.137352.27128		2.2032	2.144682.27284		2.2108	2.151522.27483	
	5	0.9941	0.967321.06936		1.0248	0.998391.10130		1.0821	1.056181.16083		1.1356	1.109941.21554	
		2.1951	2.137352.27128		2.2226	2.163692.27892		2.2800	2.218222.30846		2.3998	2.268232.35005	

* Curvilinear double taper beam.

Upon reviewing Table 12, it becomes evident that introducing variations in width influences the frequencies of the beams. Specifically, plump double-tapered beams show slightly lower frequencies compared to those with only variable thickness, whereas slender double-tapered beams exhibit a slight increase. However, the trends in frequency changes with increasing gradient index γ_e and parameter a remain consistent for both beams with only variable thickness and double-tapered beams. The frequencies increase with higher γ_e and a. This increase is more pronounced as γ_e or a become larger.

Analogously, axially graded *Type 3* plump and slender C-C beams with variable thickness and constant width, and with simultaneously variable thickness and width are examined. Table 13 presents the first two dimensionless frequencies $\bar{\omega} = \omega L\sqrt{\frac{\rho_{sus}}{E_{sus}}}$ of these beams for different values of power law parameter b and gradient index γ_c.

 doi:10.20944/preprints202407.0993.v1

It is found in Table 13 that the agreement between the results obtained from the IGA analysis in [29] and the present study is satisfactory, with errors comparable to those observed for *Type 3* plump and slender C-C beams with $b = 1$ and $\gamma_c = 1$ in Table 11. Additionally, Table 13 shows that introducing variable width along with variable height has similar effects on the frequencies of both beams with variable thickness only and curvilinearly double-tapered beams, similar to what was observed for *Type 2* plump and slender C-C beams, as mentioned earlier.

Table 13. Dimensionless natural frequencies of curvilinear taper C-C AFGM beams with various power law (4) parameters.

Model	b	0.2			0.5			0.8			1.0		
	γ_c	[29]	DTM	DTM*	[29]	DTM	DTM*	[29]	DTM	DTM*	[29]	DTM	DTM*
Plump	0	1.1029	1.10568	1.04031	1.1029	1.10568	1.04031	1.1029	1.10569	1.04031	1.1029	1.10569	1.04031
		2.3486	2.54497	2.44810	2.3486	2.54497	2.44810	2.3486	2.54498	2.44813	2.3486	2.54497	2.44813
	0.5	1.0270	1.02926	0.96840	0.9236	0.92519	0.87025	0.8254	0.82580	0.77672	0.7529	0.75141	0.70703
		2.1870	2.36872	2.27858	1.9669	2.12879	2.04736	1.7563	1.89754	1.82512	1.5969	1.72072	1.65589
	1	0.9653	0.96706	0.90989	0.8139	0.81428	0.76616	0.7002	0.69935	0.65802	0.6371	0.63543	0.59782
		2.0571	2.22708	2.14243	1.7383	1.87906	1.80811	1.4981	1.61675	1.55635	1.3641	1.47041	1.41596
	2	0.8708	0.87183	0.82031	0.6878	0.68729	0.64668	0.5897	0.58870	0.55389	0.5512	0.55024	0.51771
		1.8597	2.01193	1.93575	1.4761	1.59425	1.53483	1.2703	1.37125	1.32095	1.1901	1.28514	1.23845
	5	0.7083	0.70814	0.66630	0.5512	0.55045	0.51792	0.5044	0.50397	0.47425	0.4911	0.49077	0.46188
		1.5204	1.64301	1.58161	1.1883	1.28345	1.23660	1.0864	1.17376	1.13122	1.0551	1.13997	1.09864
Slen-der	0	0.9878	0.96659	1.06906	0.9878	0.96659	1.06906	0.9878	0.96659	1.06906	0.9878	0.96659	1.06906
		2.1970	2.15149	2.29122	2.1970	2.15149	2.29122	2.1970	2.15149	2.29122	2.1970	2.15149	2.29122
	0.5	0.9203	0.90015	0.99556	0.8285	0.81359	0.89622	0.7420	0.72427	0.80065	0.6790	0.66130	0.73109
		2.0466	2.00327	2.13265	1.8421	1.74851	1.92080	1.6476	1.60620	1.70524	1.5028	1.46410	1.54951
	1	0.8654	0.84606	0.93568	0.7309	0.71349	0.78886	0.6302	0.61411	0.67858	0.5743	0.55882	0.61731
		1.9255	1.88386	2.00444	1.6286	1.59073	1.68759	1.4054	1.37004	1.44874	1.2809	1.24838	1.31629
	2	0.7812	0.76321	0.84391	0.6183	0.60271	0.66606	0.5307	0.51674	0.57062	0.4959	0.48271	0.53300
		1.7411	1.70209	1.80889	1.3828	1.34864	1.42756	1.1895	1.15997	1.22235	1.1133	1.08328	1.14099
	5	0.6363	0.62055	0.68581	0.4955	0.48246	0.53250	0.4532	0.44121	0.48651	0.4411	0.42951	0.47381
		1.4235	1.38932	1.47301	1.1113	1.08346	1.15111	1.015	0.99219	1.06980	0.9859	0.96212	1.03009

* Curvilinear double taper beam.

On the other hand, the trends of the frequency changes with increasing b and γ_c are found to be opposite to those in *Type 2* plump and slender C-C beams. In *Type 3* plump and slender beams, the frequencies decrease with higher values of γ_c and b. This decrease begins more rapidly and exhibits a faster decay as γ_c or b increase.

Table 14. Dimensionless natural frequencies of curvilinear taper AFGM beams with various boundary conditions.

AFGM	Model	BCs	C-C			C-S			C-F			S-S		
		Mode	[29]	DTM	DTM*	[29]	DTM	DTM*	[29]	DTM	DTM*	[29]	DTM	DTM*
Type 2	Plump	1	1.1001	1.09774	1.03149	0.8392	0.83336	0.80370	0.1669	0.16736	0.16262	0.6856	0.67765	0.66811
		2	2.3377	2.51889	2.42384	1.5533	2.31624	2.25450	0.9638	1.13797	1.12997	1.8524	2.16694	2.13405
	Slender	1	0.9941	0.98513	1.06936	0.5764	0.56832	0.58619	0.1070	0.10628	0.09795	0.3468	0.34744	0.33893
		2	2.1951	2.15107	2.27128	1.7610	1.74672	1.89129	0.7314	0.7207	0.72082	1.3943	1.4032	1.43892

 doi:10.20944/preprints202407.0993.v1

Type 3	Plump	1	0.6371	0.63543	0.59782	0.5215	0.51757	0.49565	0.1460	0.14617	0.13912	0.4070	0.40223	0.39643
		2	0.8972	1.47041	1.41596	0.9537	1.36093	1.32281	0.6423	0.74588	0.73694	1.0946	1.27727	1.25659
	Slender	1	0.5743	0.55882	0.61731	0.3808	0.37381	0.39302	0.1008	0.09998	0.09508	0.2065	0.20703	0.2028
		2	1.2809	1.24838	1.31629	1.0547	1.0332	1.06555	0.4992	0.48937	0.49201	0.8293	0.82974	0.82545

* Curvilinear double taper beam.

Table 14 presents the dimensionless natural frequencies of beams with variable thickness only and curvilinearly double-tapered beams under different boundary conditions. The calculation errors for the first and second frequencies are within 3%. Notably, the second bending frequency is not available from the IGA analysis in [29] in some cases. Analyzing the data in Table 14, it is evident that the frequencies of curvilinearly double-tapered beams behave similarly to those of beams with variable thickness only, depending on the boundary conditions. In particular, the highest frequencies correspond to C-C restraints, while the lowest frequencies are observed under C-F boundary conditions.

5. Conclusions

Free vibration analysis of axially functionally graded beams with curvilinear taper cross-sections and various material distributions is performed using the semi-analytical approach of the differential transform method. Unlike standard procedure that impose boundary conditions on transformed images of unknown functions, the present DTM approach integrates various boundary conditions directly into the original continuous problem formulation. The non-uniform beam shapes, defined as conic sections, are analytically described using rational Bézier curves in the Gröbner basis in a unified manner.

The equations of motion for free vibration are derived by principle of virtual work under the assumptions of the Timoshenko beam theory. It is assumed that both the material properties of the beam and its geometric features vary continuously along the axial direction.

Comparisons are presented to validate the accuracy and assess the efficiency of the proposed computational technique. The computed examples encompass both well-documented cases and previously unexamined scenarios, ranging from uniform homogeneous and inhomogeneous beams to curvilinearly double-tapered axially functionally graded beams. In the cases, where benchmark results are unavailable in the literature, the current DTM solutions are compared with our own FEM simulations. The three-dimensional finite element modeling was conducted using the ABAQUS code with a user-defined subroutine (UMAT) to incorporate material gradients into the 3-D element C3D20.

Based on these results, the DTM in its proposed formulation exhibits excellent performance in modeling the free vibration of beams with complex geometry and material distribution. This study provides new results from frequency analysis of curvilinearly double-tapered AFGM beams. It was found that introducing simultaneous variations in height and width of the beam cross-section influences the beam's frequencies. While these changes may not be substantial, conducting accurate dynamic structural modeling remains crucial. Therefore, these findings can be useful in the design process of axially functionally graded beams and serve as benchmarks for researchers interested in exploring similar problems using alternative methods.

Author Contributions: Conceptualization, V.N.B. and R.K.; methodology, V.N.B.; software, V.N.B.; validation, V.N.B. and S.D.D.; writing—original draft preparation, V.N.B, R.K. and S.D.D.; writing—review and editing, V.N.B. and R.K. All authors have read and agreed to the published version of the manuscript.

Funding: This research received no external funding

Data Availability Statement: The raw data supporting the conclusions of this article will be made available by the authors on request.

Acknowledgments: The first author acknowledges that his research was conducted in compliance with the project of the Ministry of Education and Science of Ukraine, under grant agreement no. 0124U000975.

Conflicts of Interest: The authors declare no conflicts of interest.

 doi:10.20944/preprints202407.0993.v1

References

1. Ece, M. C.; Aydogdu, M.; Taskin V. Vibration of a variable cross-section beam. *Mech. Res. Commun.* **2007**, *34*, 78–84.
2. Zhou, D.; Cheung, Y.K. The free vibration of a type of tapered beams. *Comput. Methods Appl. Mech. Engrg.* **2000**, *188*, 203-216.
3. Caruntu, D.I. Dynamic modal characteristics of transverse vibrations of cantilevers of parabolic thickness. *Mech. Res. Commun.* **2009**, *36*, 391-404.
4. Burlayenko, V.N.; Sadowski, T. Dynamic analysis of debonded sandwich plates with flexible core – Numerical aspects and simulation. In *Shell-like Structures*; Altenbach, H.; Eremeyev, V., Eds.; Springer: Berlin, Heidelberg, 2011; *Adv. Struct. Mater.* Vol. 15, pp. 415–440.
5. Burlayenko, V.N.; Altenbach, H.; Sadowski, T. Dynamic fracture analysis of sandwich composites with face sheet/core debond by the finite element method. In *Dynamical Processes in Generalized Continua and Structures*; Altenbach, H.; Belyaev, A.; Eremeyev, V.; et al., Eds.; Springer: Cham, 2019; *Adv. Struct. Mater*. Vol 103, pp. 163 – 194.
6. Carrera, E.; Demirbas, M.D.; Augello, R. Evaluation of stress distribution of isotropic, composite, and FG beams with different geometries in nonlinear regime via Carrera-unified formulation and Lagrange polynomial expansions. *Appl. Sci.* **2021**, *11*, 10627.
7. Elishakoff I. *Eigenvalues of Inhomogenous Structures: Unusual Closed-form Solutions*. CRC Press: New York, 2005.
8. Yuan, J.;·Pao, Y.-H.;·Chen, W. Exact solutions for free vibrations of axially inhomogeneous Timoshenko beams with variable cross section. *Acta. Mech.* **2016**, *227*, 2625–2643.
9. Zhao, Y.; Huang, Y.; Guo, M. A novel approach for free vibration of axially functionally graded beams with non-uniform cross-section based on Chebyshev polynomials theory. *Compos. Struct.* **2017**, *168*, 277-284.
10. Xie, X.; Zheng, H.; Zou, X. An integrated spectral collocation approach for the static and free vibration analyses of axially functionally graded nonuniform beams. *Proc. Inst. Mech. Eng., Part C* **2017**, *231*(13), 2459-2471.
11. Chen, W.-R. Vibration analysis of axially functionally graded Timoshenko beams with non-uniform cross-section. *Lat. Am. J. Solids Struct.* **2021**, *18*(07), 1-18.
12. Zhang, X.F.; Zhuang, Y.; Zhou Y.J.J. A Jacobi polynomial based approximation for free vibration analysis of axially functionally graded material beams. *Comput. Struct.* **2019**, *225*, 111070.
13. Cao, D.X.; Wang, J.J.; Gao, Y.H. et al. Free vibration of variable width beam: asymptotic analysis with FEM simulation and experiment confirmation. *J. Vib. Eng. Technol.* **2019**, *7*, 235–240.
14. Ghazaryan, D.; Burlayenko, V.N.; Avetisyan, A.; Bhaskar, A. Free vibration analysis of functionally graded beams with non-uniform cross-section using the differential transform method. *J. Eng. Math.* **2018**, *110*, 97–121.
15. Rajasekaran, S.; Tochaei, E.N. Free vibration analysis of axially functionally graded tapered Timoshenko beams using differential transformation element method and differential quadrature element method of lowest-order. *Meccanica* **2014**, *49*, 995–1009.
16. Keshmiri, A.; Wu, N.; Wang, Q. Free vibration analysis of a nonlinearly tapered cone beam by Adomian decomposition method. *Int. J. Struct. Stab. Dyn.* **2018**, *18*(07), 1850101.
17. Lin, M.-X.; Deng, C.-Y.; Chen, C.-K. Free vibration analysis of non-uniform Bernoulli beam by using Laplace Adomian decomposition method. *Proc. Inst. Mech. Eng., Part C* **2022**, *236*(13), 7068-7078.
18. Wang, P.; Wu, N.; Sun, Z.; Luo, H. Vibration and reliability analysis of non-uniform composite beam under random load. *Appl. Sci.* **2022**, *12*, 2700.
19. Mahmoud, M. Natural frequency of axially functionally graded, tapered cantilever beams with tip masses. *Eng. Struct.* **2019**, *187*, 34–42.
20. Chen, Y.; Dong, S.; Zang, Z; et al. Free transverse vibrational analysis of axially functionally graded tapered beams via the variational iteration approach. *J. Vib. Control* **2021**, *27*(11-12), 1265-1280.
21. Liu, X.; Chang, L.; Banerjee, J.R.; Dan, H.-C. Closed-form dynamic stiffness formulation for exact modal analysis of tapered and functionally graded beams and their assemblies. *Int. J. Mech. Sci.* **2022**, *214*, 106887.
22. Adelkhani, R.; Ghanbari, J. Vibration analysis of nonlinear tapered functionally graded beams using point collocation method. *Int. J. Comput. Methods Eng. Sci.* **2022**, *23*(4), 334-348.
23. Kumar, S.; Mitra, A.; Roy, H. Geometrically nonlinear free vibration analysis of axially functionally graded taper beams. *Eng. Sci. Technol. Int. J.* **2015**, *18*, 579 – 593.

24. Ghayesh, M.H. Nonlinear vibration analysis of axially functionally graded shear-deformable tapered beams. *Appl. Math. Model.* **2018**, *59*, 583–596.
25. Soltani, M.; Asgarian, B. New hybrid approach for free vibration and stability analyses of axially functionally graded Euler-Bernoulli beams with variable cross-section resting on uniform Winkler-Pasternak foundation. *Lat. Am. J. Solids Struct.* **2019**, *16*(3), 1-25.
26. Singh, R.; Sharma, P. Vibration analysis of an axially functionally graded material non-prismatic beam under axial thermal variation in humid environment. *J. Vib. Control* **2022**, *28*(23-24), 3608-3621.
27. Özdemir, Ö. Vibration and buckling analyses of rotating axially functionally graded nonuniform beams. *J. Vib. Eng. Technol.* **2022**, *10*, 1381–1397.
28. Bazoune, A. Free vibration frequencies of a variable cross-section Timoshenko-Ehrenfest beam using Fourier-p element. *Arab. J. Sci. Eng*. **2024**, *49*, 2831–2851.
29. Chen, M.; Jin, G.; Zhang, Y.; Niu, F.; Liu, Z. Three-dimensional vibration analysis of beams with axial functionally graded materials and variable thickness. *Compos. Struct.* **2019**, *207*, 304–322.
30. Valencia Murillo, C.E.; Gutierrez Rivera, M.E.; Flores Samano, N.; Celaya Garcia, L.D. A seven-parameter spectral/hp finite element model for the linear vibration analysis of functionally graded shells with nonuniform thickness. *Appl. Sci.* **2023**, *13*, 11540.
31. Burlayenko, V.N.; Kouhia, R.; Dimitrova, S.D. One-dimensional vs. three-dimensional models in free vibration analysis of axially functionally graded beams with non-uniform cross-sections. *Mech. Compos. Mater*. **2024**, *60*, 83–102.
32. Burlayenko, V.N. Modelling thermal shock in functionally graded plates with finite element method. *Adv. Mater. Sci. Eng.* **2016**, *2016*, 7514638, 1-12.
33. Burlayenko, V.N.; Dimitrova, S.D.; Altenbach, H. A material model-based finite element free vibration analysis of one-, two- and three-dimensional axially FGM beams. In Proceedings of Conference 2021 IEEE KhPI Week on Advanced Technology, Kharkiv, Ukraine, 13 – 17 September 2021; pp. 628-633.
34. Burlayenko, V.N. A continuum shell element in layerwise models for free vibration analysis of FGM sandwich panels. *Continuum Mech. Thermodyn.* **2021**, *33*, 1385–1407.
35. Lee, J.K., Lee, B.K. Coupled flexural-torsional free vibration of an axially functionally graded circular curved beam. *Mech. Compos. Mater.* **2022**, *57*, 833–846.
36. Rezaiee-Pajand, M., Masoodi, A.R. & Alepaighambar, A. Lateral-torsional buckling of a bidirectional exponentially graded thin-walled C-shaped beam. *Mech. Compos. Mater.* **2022**, *58*, 53–68
37. Liu, P.; Tang, J.; Jiang, B.; Li, Y. Nonlinear parametric vibration analysis of the rotating thin-walled functionally graded material hyperbolic beams. *Math. Meth. Appl. Sci.* **2024**, *47*, 2952–2965.
38. Chen, W. R.; Chang H. Closed-form solutions for free vibration frequencies of functionally graded Euler-Bernoulli beams. *Mech. Compos. Mater.* **2017**, *53*, 79-98.
39. Martin, B.; Salehian, A. Techniques for approximating a spatially varying Euler-Bernoulli model with a constant coefficient model. *Appl. Math. Model.* **2020**, *79*, 260–283.
40. Rao, S.S. *Mechanical Vibrations*, 4th ed.; Person Prentice Hall: New York, 2004.
41. Piegl, L; Tiller, W. Conies and Circles. In *The NURBS books*, 2nd ed.; Springer-Verlag: Berlin Heidelberg, 1995; pp. 281-331.
42. Anwar,Y. R.; Tasman, H.; Hariadi, N. Determining implicit equation of conic section from quadratic rational Bézier curve using Gröbner basis. *J. Phys.: Conf. Ser.* **2021**, *2106*, 012017.
43. Pukhov, G. E. *Differential Transformations and Mathematical Modeling of Physical Processes*. Naukova Dumka: Kiev, Ukraine, 1986.
44. Burlayenko, V.N.; Altenbach, H.; Dimitrova, S.D. Modal characteristics of functionally graded porous Timoshenko beams with variable cross-sections. Compos.Struct. **2024**, *342*, 118273.
45. MATLAB version: 9.1.0 (R2016b), The MathWorks Inc., Natick, Massachusetts, United States, 2016. URL https://www.mathworks.com.
46. ABAQUS User's Manual, Version 2016. Dassault Systèmes Simulia Corp., Providence, RI, USA, 2016.

Zhou, H.; Ling, M.; Yin, Y.; Hu, H.; Wu, S. Exact vibration solution for three versions of Timoshenko beam theory: A unified dynamic stiffness matrix method. *J. Vib. Control.* **2023**, 1-15.